ISSN 1330-3651 (Print), ISSN 1848-6339 (Online) https://doi.org/10.17559/TV-20230117000231
Preliminary communications

Design of an Air-Assisted Mechanical Seed-Metering Device for Millet (Setaria Italica) Based on Experiments and Simulation Analysis

Qianwen KOU, Lingxin BU*, Jun CHEN, Adilet SUGIRBAY

Abstract: In this study, an air-assisted mechanical seed-metering device for millet (Setariaitalica) was developed. The discrete element method (DEM) and response surface method (RSM) were used to research the influences of the side length, depth, and oblique angle of the shaped hole on the seeding performance (quality, multiples, and miss indices) of the seed-metering device, and the parameters of the shaped hole were optimized. Furthermore, after determining the size of the shaped hole, the influence of negative pressure on the quality index was studied under the condition of the higher rotational speed of the seed-sowing wheel. At the rotational speed of 20 r/min, the optimal values of the side length, depth, and oblique angle of the shaped hole were found to be 3.55 mm, 2.1 mm, and 109°, which resulted in a quality index of 94%. The optimal parameters were consistent with the simulated values and bench test values, with a relative deviation of 5.05%. Moreover, under the condition of a rotational speed of 40 r/min, the application of appropriate negative pressure to the seeds was found to promote seed entry into the shaped hole, thus significantly reducing the miss index and increasing the quality index. At the negative pressure of −90 Pa, the quality index was found to exceed 90%. These results provide a theoretical basis for future studies on a seed-metering device for millet (Setaria italica).

Keywords: DEM modeling; millet (Setaria italic); precision metering; quality index; seed-metering device

1 INTRODUCTION

Compared with other crops, millet (Setaria italica) has more advantages in health and other aspects; for example, its polyphenol, vitamin E, vitamin B1, and vitamin B2 contents are higher than those of wheat and other major grain crops [1]. The size of millet seeds in three dimensions is very small; it is thus difficult to control the number of seeds during the planting process, which leads to low planting quality and outputs. The difficulty in realizing precision seeding introduces challenges to the planting and industrialization of millet [2]. The planting quality is usually determined by the seed-metering device, which can be mechanical, pneumatic, or pneumatic-mechanical. Although many scholars have carried out numerous investigations and explorations of seed-metering devices for small seeds, a mature seed-metering device that can meet the requirements of millet has not emerged [3]. The exploration of mechanical seed sowers for small grains has mainly focused on structural improvements to make them more suitable for the planting pattern of small grains. Zhang et al. designed a new multifunctional seed sower for the precision sowing of small seed crops, and a new precision seeder with a mechanical structure for pushing seeds out of the seeder was developed for a variety of small seed diameters. Moreover, a pusher wheel engages with the seed sowing hole to squeeze out the seeds to achieve seeding, and different combinations of the seed sowing wheel and pusher wheel can be assembled according to different seeds [4]. Xie et al. conducted a bench test with a nested wheel seeder to find the best working parameters when seeding small seed crops, such as cereals and rape. In response to the phenomenon of poor seeding quality when using a nested wheel seeder for precision sowing, they provided a new idea for the adaptation of the nested wheel seeder to the sowing of small seed crops [5]. The removal of seeds adsorbed on the air holes of pneumatic seed dispensers by mechanical or pneumatic means is an important research direction for pneumatic dispensers of small seeds, and the exploration of a way to clear the seeds from the air holes is particularly significant [6]. Zhang et al. added a cleaning device to the pneumatic seed discharger. This structure has a better cleaning effect for seeds adsorbed on air holes, and the air holes are not easily blocked. However, it does not fundamentally solve the sowing leakage produced by the pneumatic seed discharger [7]. Kang et al. (2020) adopted a combination of pneumatic and mechanical methods to remove the adsorbed seeds at the stomata, and used the structure of a pressure separator to reduce the negative-pressure air chamber and improve the seed-blowing efficiency. They designed a mechanical seed-cleaning device to clean the seeds blocked in the stomata. The test results showed that the qualified rate could reach 93.2%, which is greater than the national standard of a pass rate of more than 80% [8]. On the basis of pneumatic and mechanical seed dispersers, increasingly more scholars have deeply explored some pneumatic-mechanical composite seed dispersers. Mechanical seed dispersers are reliable but have low efficiency, and while pneumatic seed dispersers have high efficiency, the sowing effect depends entirely on the pneumatic force. Moreover, pneumatic suction-based seed dispersers are prone to the blockage of the suction hole, leading to increases in negative pressure plunge and the leakage rate during the working process. Based on these characteristics, Jia et al. developed a new type of soybean precision seeder by combining pneumatic force with a mechanical seed-filling device. The seeds can be sent to the air holes with suction force by moving along the mechanical seed guide groove, and the seeds are adsorbed on the air holes under the joint action of the mechanical structure and pneumatic attraction. This improves the quality of seed filling [9]. In summary, domestic scholars have achieved fruitful results based on the extensive research of seed sowers for small seed crops. However, the following problems still exist. First, while mechanical seed sowers can achieve a better sowing effect at a lower working speed, they are not suitable for higher-speed sowing operations. Moreover, air-absorbing seed sowers depend on the vacuum size of the air chamber, which will lead to a sudden decrease in sowing quality when seed blockage occurs. Pneumatic-mechanical composite seeders

mostly use mechanical guidance or the mechanical structure to assist the pneumatic seeding, which is more suitable for small seed crops such as rape that require singular seeding. However, the agronomic requirements of multi-grain hole sowing lead to an increase in the complexity of the auxiliary structure and poor results. Most pneumatic-mechanical composite seeders only achieve certain results for this part of the seeding, and the new seeders are less often used. Therefore, this study is aimed at the design of an air suction-assisted mechanical seed-metering device for millet (Setaria italica). Its structure is optimized based on simulation tests, and its performance is evaluated via laboratory bench tests.

2 MATERIALS AND METHODS

2.1 Design Requirements

Millet (Setaria italica) is a small seed crop. The highest yield is achieved when the number of seedlings left in a single cereal plant is 1 - 3, and the yield begins to decrease when the number exceeds 3. Moreover, the number of seeds sown per hole has no significant effect on the seeding rate. According to the agronomic requirements of cereal sowing, the air suction-assisted mechanical cereal seeder designed in this study should meet the sowing requirements of 2 - 3 seeds per hole.

2.2 Parameter Measurement

In this study, Jingu 21 was used as the research object, and 500 seeds were graded and randomly selected to measure the three axes of the grain length, width, and height. The dimensions were measured using an electronic vernier caliper with an accuracy of 0.02 mm, and the measurement results were counted and analyzed, as exhibited in Tab. 1.

Table 1 The triaxial sizes of millet

Parameter	Mean	Standard deviation	Size range
L / mm	2.03	0.45	1.95 - 2.14
W / mm	1.44	0.26	1.37 - 1.56
T / mm	1.86	0.21	1.77 - 1.92
Weight of one thousand seeds / g	26.455		

2.3 Structure and Working Principle of the Seed-Sowing Device

As depicted in Fig. 1, the air suction-assisted mechanical seed-metering device mainly consists of two shells (1 and 2), a seed-sowing wheel (3), two fluorine rubber seal rings (4) fixed on the rotating shaft, deep-groove ball bearings (5), an air box (6), a brush (7), and a closed air suction chamber. The air box (6) and shells (1 and 2) are fixed to the frame, and deep-groove ball bearings (5) make the seed-sowing wheel (3) rotate relative to the air box (4). Shaped holes on the seed-sowing wheel (3) are connected with the air suction chamber through channels, so that negative pressure acts on the seeds in the shaped holes, and two fluorine rubber seal rings (4) ensure the air tightness of the air suction chamber.

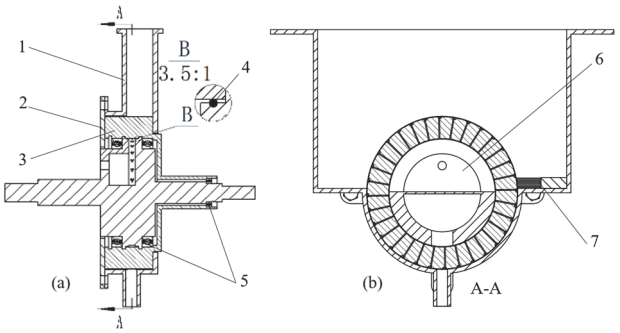

Figure 1 The structure of the seed-metering device: (a) the cross-section of the main view of the device; (b) the cross-section of the side view of the device

As shown in Fig. 2, a complete seed release mainly includes four steps: seed filling, seed cleaning, seed protection, and seed feeding. In the seed-filling stage, the seeds enter the shaped holes distributed in the seed-sowing wheel under the action of their own gravity, inter-seed force, and air suction. The size of the shaped holes makes it impossible for a fourth grain to enter, while the negative pressure further fixes the seeds in the holes. When the shaped hole is rotated to the position of the seed-cleaning brush, the brush scrapes away the grains that have not entered the hole. When the seeds in the shaped hole enter the seed protection area, the shells block the grain so that the seeds cannot fall out of the hole. Finally, when the seeds reach the seed-sowing area, the seeds leave the seed-metering device under the action of their own weight and centrifugal force to complete a seed discharge.

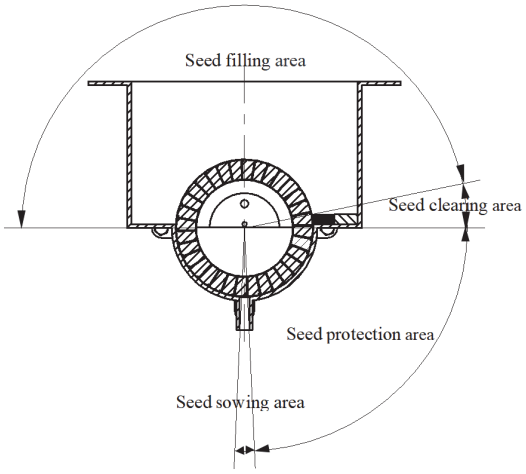

Figure 2 The working principle of the seed-metering device

2.4 Design of the Main Components

2.4.1 Structural Design of the Seed-Sowing Wheel

As shown in Fig. 3, one end of the seed-sowing wheel is the drive shaft, which is used for the driving of the wheel, and the inside of the wheel is a hollow structure, which is used to cooperate with the air box. The diameter of the seed-sowing wheel, the diameter of the drive shaft, and the thickness of the seed-sowing wheel are 140, 64, and 20 mm, respectively. Moreover, the surface of the seed-sowing wheel is evenly distributed with three triangular air channels at the bottom of each shaped hole to connect it with the air box. To ensure that the seeds will not fall into the air channel, its diameter was determined to be 1 mm

according to the measured size of the three axes of the seeds.

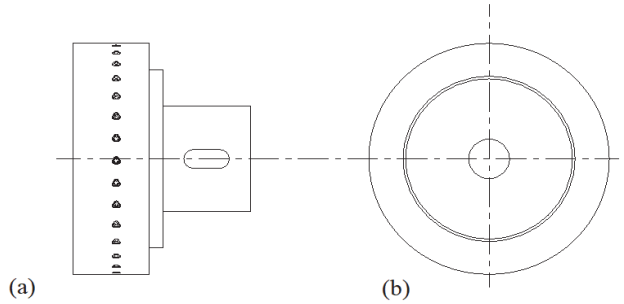

Figure 3 The structure of the seed-sowing wheel: (a) main view; (b) side view

2.4.2 Structural Design of the Air Box

As shown in Fig. 4, there is an air hole on one side of the air box to mount an air tube to connect the vacuum generator to generate negative pressure. The upper part of the air box has an opening positioned opposite to the seed-filling area of the seed-metering device to ensure the maximum area for air suction-assisted seed filling. The shafts at each end of the air box are fitted with a bearing and a seal to ensure good air tightness.

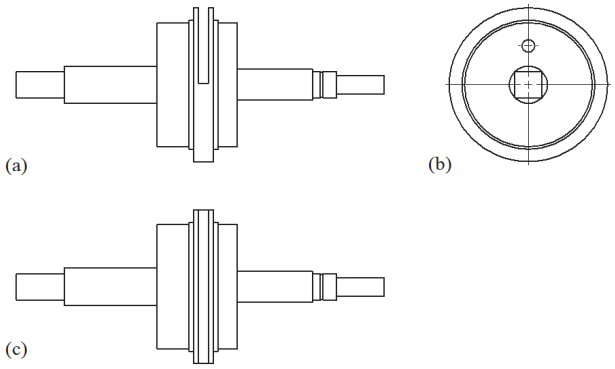

Figure 4 The structure of the air box: (a) main view; (b) side view; (b) vertical view

2.4.3 Determination of the Size of the Shaped Hole of the Seed-Sowing Wheel

The size of the shaped hole is crucial for the sowing effectiveness [10]. To ensure a good sowing effect, the side length of the shaped hole should be no less than $1.2d_{max}$ and no more than $2d_{min}$ of the maximum diameter of the seed arrangement. Based on the agronomic requirements, the shaped hole is designed as an inverted trapezoid with rounded triangles to fill three seeds, which is conducive to the smooth discharge of seeds during the seed-sowing process, as shown in Fig. 5a. To fill each shaped hole with 2 - 3 seeds, the cleaning brush removes the seeds that do not enter the hole. However, for the case in which the shaped hole is filled with three seeds, if more than one-half of the fourth seed enters the hole, the fourth seed has a higher probability of squeezing into the hole; thus, the parameter of the hole could accommodate a maximum of one-half of the volume of the fourth seed [11]. Moreover, there are three air channels with a 1 mm diameter at the bottom of each shaped hole. The concave surface created by the air channels running through the bottom of the shaped hole can more easily move the position of the center of gravity of the seeds filling the hole to the air channel position, thus limiting the fourth seed from entering the hole.

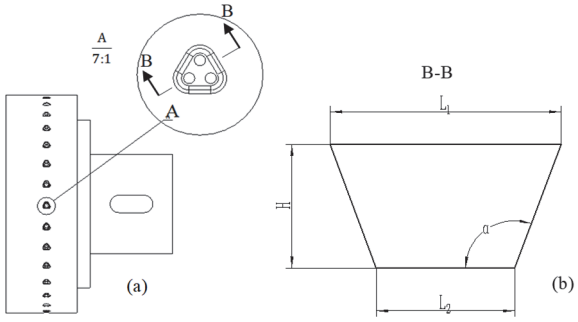

Figure 5 The structure of the shaped hole: (a) enlarged view; (b) section

According to a previous research report [12], the relationship Eq. (1) and Eq. (2) can respectively be used to determine the side length (D) and the hole depth (H):

$$1.3d_{max} > D > 1.1d_{min} \tag{1}$$

$$1.1h_{max} > H > 0.9h_{min} \tag{2}$$

where D is the side length (mm), d_{max} is the maximum value range of the side length (mm), d_{min} is the minimum value range of the side length (mm), H is the hole depth (mm), h_{max} is the minimum value range of the side depth (mm), and h_{min} is the minimum value range of the side depth (mm).

According to the data reported in Tab. 1, the sizes of the three axes of the seeds are similar, ranging from 1.37 to 2.14 mm. When a hole is filled with three seeds, as shown in Fig. 6a, 3.01 mm < d_1 < 5.56 mm and 1.23 mm < H < 2.35 mm are obtained according to Eq. (1) and Eq. (2). Similarly, when the hole shown in Fig. 7b can be filled with four seeds, 3.74 mm < d_2 < 5.85 mm.

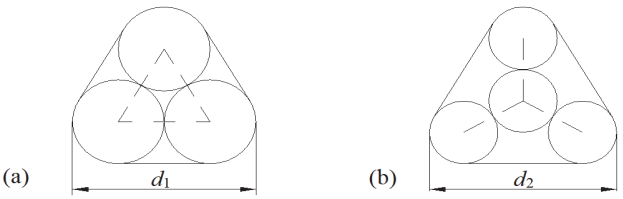

Figure 6 The arrangement of seeds in the hole: (a) three seeds; (b) four seeds

Also, as analyzed previously, the slope of the shaped hole should be considered an important parameter, as a large slope will result in excess seed filling caused by the large value of L_1, as shown in Fig. 6b. Therefore, L_1 can be calculated as follows:

$$L_1 = 2H\tan\left(\alpha - \frac{\pi}{2}\right) + L_2 \tag{3}$$

where L_1 and L_2 are respectively the lengths of the upper and bottom sides of the shaped hole (mm), H is the depth of the shaped hole (mm), and α is the oblique angle of the shaped hole (degrees).

In the process of seed filling, to prevent the fourth seed from entering the shaped hole (as shown in Fig. 7b), the size of the shaped hole should meet the following conditions: 3.01 mm < L_2 < 3.74 mm, L_1 < 5.56 mm, and 1.23 mm < H <2.35 mm. Therefore, according to Eq. (3), the range of the oblique angle of the shaped hole α is 90° < α < 119°. The values of these parameters must be further obtained through simulation analysis.

2.4.4 Determination of the Number of Shaped Holes on the Seed-Sowing Wheel

According to a previous report [12], the number of shaped holes on the seed-sowing wheel has a significant influence on seed filling, and can be calculated as follows:

$$z = \frac{\pi d(1+\delta)v_m}{v_P s} \tag{4}$$

where z is the number of shaped holes on the seed-sowing wheel, d is the diameter of the seed-sowing wheel (m), δ is the slip coefficient of the planter, the value range of which is from 0.05% to 0.12%, v_m is the working speed of the planter (m/s), v_P is the linear speed of the seed-sowing wheel (m/s), and s is the seed spacing (m).

In this study, the parameters were designed as follows: d = 0.14 m, s = 0.016 m, v_m = 0.15 m/s, and v_P = 0.147 m/s (20 r/min). Thus, the number of shaped holes was calculated as $z \approx 37$.

2.5 Development of the Discrete Element Model

To verify the feasibility of the seed-metering device and optimize the parameters, EDEM software was used to simulate the filling and seeding processes via the discrete element method (DEM). The seed-metering device model was established with Solidworks 2018 software, converted into. igs format, and imported into EDEM software [13]. The shells, seed-sowing wheel and air box of seed-metering device were 3-D printed from resin materials. The seed model consisted of seven cell balls, the diameter and center coordinates of which were explicit, as shown in Fig. 7 [14].

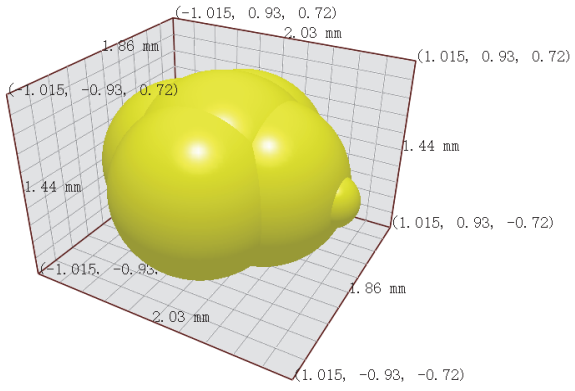

Figure 7 The seed model in EDEM

In the particle factory, the particles were set as having a normal distribution, and the mean value, standard deviation, upper limit, and lower limit of the particles were set as 1, 2.5, 1.1, and 0.9, respectively. The Hertz-Mindlin (no-slip) contact model was adopted because there was no adhesion force on the seed surface [15]. In addition, in the simulation experiment, a total of 5000 seeds were generated. The rotation speed of the seed-sowing wheel was set as 20 r/min, and the simulation time was 27 s with a step size of 1e−4 s. Other simulation parameters are listed in Tab. 2, and the seeding process is depicted in Fig.8.

Table 2 The model parameters used in the simulations

Identity	Property	Value
Seed	Density / kg/m^3	1267
	Shear modulus / Pa	1×10^8
	Poisson's ratio	0.25
Resin	Density / kg/m^3	1385
	Shear modulus / Pa	1.35×10^8
	Poisson's ratio	0.4
Seed-seed	Coefficient of restitution	0.55
	Dynamic friction coefficient	0.51
	Rolling friction coefficient	0.06
Seed- resin	Coefficient of restitution	0.52
	Dynamic friction coefficient	0.5
	Rolling friction coefficient	0.05

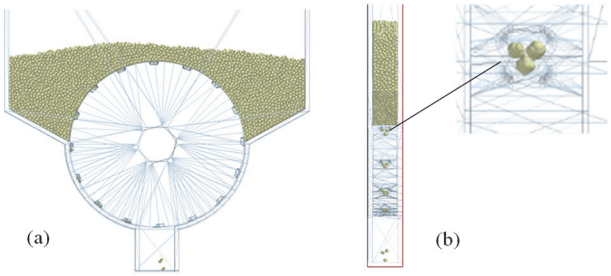

Figure 8 The EDEM models of the (a) seed-metering device and (b) seeding process

2.6 Simulation Experiment Design

To determine the influences of the depth H, the side length D_2, and the oblique angle α of the shaped hole on the seeding process, the Box-Behnken design with three levels was applied for these three factors and implemented using Design-Expert 8.0. The factor codes are listed in Tab. 3. The response surface method (RSM) was applied to define the correlations between the responses and the control factors. The response variable could be fitted into the general form of a quadratic polynomial model, as follows [16]:

$$Y = \beta_0 + \sum_{i=1}^{3}\beta_i X_i + \sum_{i=1}^{3}\beta_{ii} X_i^2 + \sum_{i=1}^{2}\sum_{j=i+1}^{3}\beta_{ij} X_i X_j \tag{5}$$

where Y is the response variable measured for each combination of the factorial level, and β_0, β_i, β_{ii}, and β_{ij} are the regression coefficients for the intercept, linearity, square, and interaction, respectively.

Table 3 The factor codes of the independent variable levels

Factor	Unit	−1	0	1
Bottom side length of shaped hole, L_2 (X_1)	mm	3.50	3.55	3.60
Depth of the shaped hole, H (X_2)	mm	2.05	2.10	2.15
Oblique angle of the shaped hole, α	°	108	109	110

2.7 Laboratory Bench Test

With the optimal contributing factors as design parameters, a seed-metering device was fabricated and tested on a bench tester. As shown in Fig. 9, the seed-metering device was mounted on the base frame, and was driven by a motor through a synchronous belt. To test the influence of negative pressure on seeding, one end of the air tube was connected to the air box of the seed-metering device, and the other end was connected to an air compressor via a vacuum generator. The negative pressure was controlled by a vacuum pressure-regulating valve (IRV10-C06, (−100) −0 kPa, Wenzhou, Zhejiang, China), and the rotational speed of the seed-sowing wheel was measured by an SW-6234C laser speed-measuring instrument (Suwei, Guangzhou, Guangdong, China).

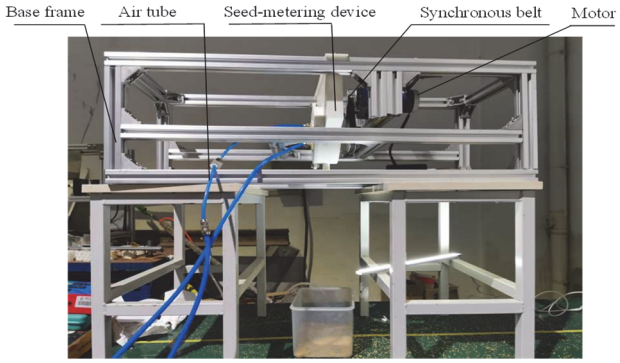

Figure 9 The bench test of the air-assisted millet seed-sowing device

2.8 Performance Indicators

There are three performance indicators of a seed-sowing device, namely the quality index, the multiples index, and the miss index [17]. "Normal" was considered the discharge of two or three seeds from the discharge spout; a "miss" was considered the discharge of fewer than two seeds; the discharge of more than three seeds at a time was considered "multiple. " The multiples, miss, and quality indices were defined as the percentages of the multiple, miss, and normal operations, and were calculated using the following equations:

$$\begin{cases} I_C = \dfrac{Z_1}{Z} \\ I_L = \dfrac{Z_2}{Z} \\ I_H = 1 - I_C - I_L \end{cases} \tag{6}$$

where I_C is the multiples index, I_L is the miss index, I_H is the quality index, Z_1 and Z_2 are the counts of multiples and misses, respectively, and Z is the theoretical number of total seed discharges.

3 RESULTS AND DISCUSSION

3.1 Multi-Factor Simulation Test

A total of 17 testing groups were set up in the simulation experiment. The response variables Y_1, Y_2 and Y_3 were the quality, multiples, and miss indices, respectively. The experimental schemes and results are reported in Tab. 4.

Table 4 The experimental design comprising three independent variables at three levels, and the simulation results of the responses

	X_1	X_2	X_3	Y_1	Y_2	Y_3
1	−1	−1	0	97.33	0	2.67
2	1	−1	0	98.33	1.00	0.67
3	−1	1	0	98.00	0	2.00
4	1	1	0	98.33	1.67	0
5	−1	0	−1	97.00	0	3.00
6	1	0	−1	98.33	1.00	0.67
7	−1	0	1	98.33	0	1.67
8	1	0	1	98.00	2.00	0
9	0	−1	−1	97.67	0	2.33
10	0	1	−1	98.33	0	1.67
11	0	−1	1	98.33	0.67	1.00
12	0	1	1	98.34	1.33	0.33
13	0	0	0	99.00	0	1.00
14	0	0	0	99.33	0	0.67
15	0	0	0	99.00	0.33	0.67
16	0	0	0	99.00	0.33	0.67
17	0	0	0	98.67	0.00	1.33

3.1.1 Response Surface Analysis of the Quality Index (Y_1)

Tab. 5 reports the analysis of variance (ANOVA) results used to evaluate the quadratic model. It can be seen that X_1, X_3, X_1, X_3, X_1^2, X_2^2, and X_3^2 were found to have significant effects ($p < 0.05$) on the quality index. The coefficients of the quality index model responses using the factor codes as variables can be expressed as follows.

$$\begin{aligned} Y_1 = {} & 98.98 + 0.28X_1 + 0.16X_2 + 0.20X_3 \\ & -0.16X_1X_2 - 0.40X_1X_3 - 0.16X_2X_3 \\ & -0.57{X_1}^2 - 0.33{X_2}^2 - 0.41X_3^2 \end{aligned} \tag{7}$$

Table 5 The ANOVA results of the quadratic model response to the quality index

Items	Sum of squares	DOF	Mean square	F-value	p-value
Model	4.78	9	0.53	11.91	0.0018**
X_1	0.63	1	0.63	14.06	0.0072**
X_2	0.2	1	0.20	4.59	0.0694
X_3	0.32	1	0.32	7.17	0.0316*
$X_1 X_2$	0.1	1	0.10	2.30	0.1736
$X_1 X_3$	0.64	1	0.64	14.34	0.0068**
$X_2 X_3$	0.1	1	0.10	2.30	0.1736
X_1^2	1.36	1	1.36	30.45	0.0009**
X_2^2	0.45	1	0.45	10.15	0.0154*
X_3^2	0.7	1	0.70	15.71	0.0054**
Residual	0.31	7	0.045		
Lack of fit	0.026	3	8.53e −03	0.12	0.9442
Pure error	0.29	4	0.072		

The RSM was used to analyze the interaction effects of the side length, depth, and oblique angle of the shaped hole on the quality index. As shown in Fig. 10a, the interaction between the side length and depth of the shaped hole was found to have a significant influence on the quality index. Given a depth of the shaped hole, the quality index was found to first increase and then decrease with the increase of the side length of the shaped hole. This is because a short side length causes the shaped hole to be too small to accommodate more than two seeds; however, a long side length will lead to excess seeds in the shaped hole. Furthermore, given a side length of the shaped hole, the quality index was found to first increase and then

decrease with the increase of the depth of the shaped hole. When the depth of the shaped hole is insufficient, the seeds are easily removed by the brush, resulting in missing seeding; when the depth of the hole is too large, the seeds may be superimposed in two layers in the shaped hole. Moreover, Fig. 10b reveals that the influence of the side length of the shaped hole on the quality index is greater than the influence of the oblique angle, and Fig. 10c shows that the influence of the oblique angle of the shaped hole on the quality index is slightly greater than the depth.

3.1.2 Response Surface Analysis of the Multiples Index (Y_2)

Tab. 6 reports the ANOVA results used to evaluate the quadratic model. It can be seen that X_1, X_2, X_3, X_1X_3 and X_1^2 exhibited significant effects ($p < 0.05$) on the multiples index. The coefficients of the multiples index model responses using the factor codes as variables can be expressed as follows.

$$\begin{aligned} Y_2 = {} & 0.13 + 0.68X_1 + 0.16X_2 + 0.36X_3 \\ & + 0.16X_1X_2 + 0.24X_1X_3 + 0.16X_2X_3 \\ & + 0.38X_1^2 + 0.14X_2^2 + 0.22X_3^2 \end{aligned} \quad (8)$$

As shown in Fig. 11a, the interaction between the side length and depth of the shaped hole was found to have a significant influence on the multiples index, and the multiples index was the lowest when both the oblique angle and depth of the shaped hole were at low levels. In terms of Fig. 11b, given a depth of the shaped hole, the multiples index was found to increase rapidly with the increase of the side length of the shaped hole. Furthermore, given a side length of the shaped hole, the depth of the shaped hole was found to have little effect on the multiples index. Moreover, Fig. 11c shows that the multiples index was the lowest when both the depth and oblique angle of the shaped hole were at low levels.

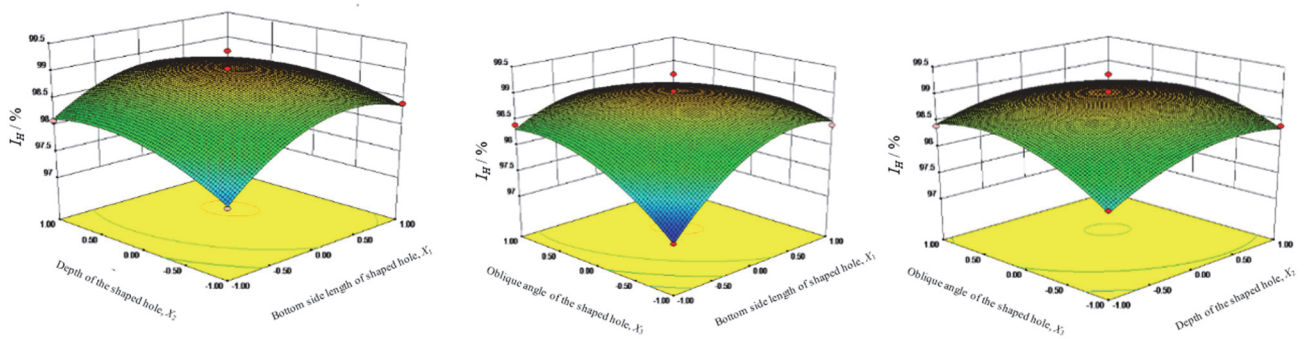

(a) (b) (c)

Figure 10 The response surfaces of the effects of interactive factors on the quality index

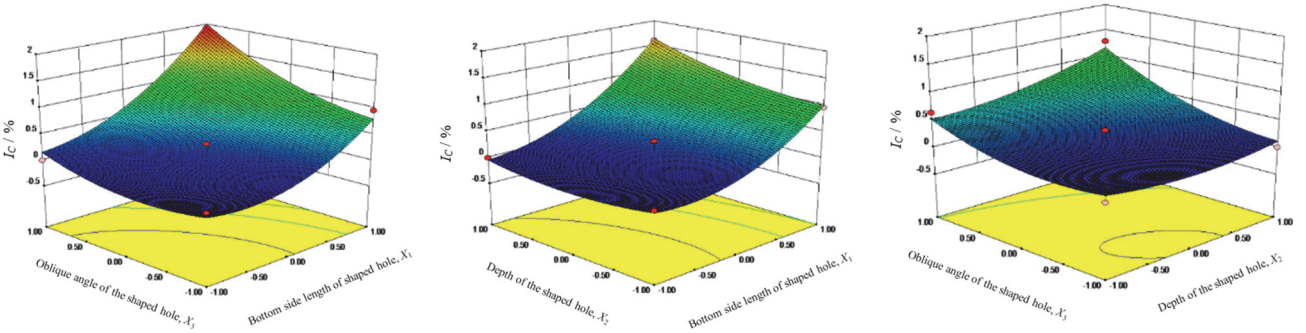

(a) (b) (c)

Figure 11 The response surfaces of the effects of interactive factors on the multiples index

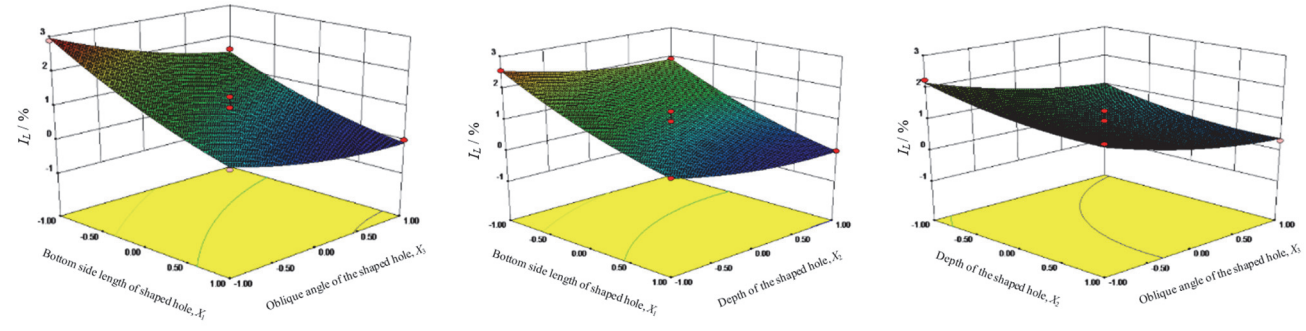

(a) (b) (c)

Figure 12 The response surfaces of the effects of interactive factors on the miss index

Table 6 The ANOVA results of the quadratic model response to the multiples index

Items	Sum of squares	DOF	Mean square	*F*-value	*p*-value
Model	6.33	9	0.700	19.61	0.0004***
X_1	3.7	1	3.700	103.21	< 0.0001***
X_2	0.2	1	0.200	5.71	0.0481*
X_3	1.04	1	1.040	28.93	0.001**
$X_1 X_2$	0.1	1	0.100	2.86	0.1348
$X_1 X_3$	0.23	1	0.230	6.43	0.0389*
$X_2 X_3$	0.1	1	0.100	2.86	0.1348
X_1^2	0.6	1	0.600	16.61	0.0047**
X_2^2	0.078	1	0.078	2.17	0.184
X_3^2	0.2	1	0.200	5.48	0.0518
Residual	0.25	7	0.036		
Lack of fit	0.13	3	0.043	1.39	0.3678
Pure error	0.12	4	0.031		

3.1.3 Response Surface Analysis of the Miss Index (Y_3)

Tab. 7 reports the ANOVA results used to evaluate the quadratic model. It can be seen that X_1, X_2, and X_3 were found to have significant effects ($p < 0.05$) on the multiples index. The coefficients of the miss index model responses using the factor codes as variables can be expressed as follows.

$$Y_3 = 0.90 - 0.96X_1 - 0.32X_2 - 0.56X_3 + \\ +0.16X_1X_3 + 0.19X_1^2 + 0.19X_2^2 + 0.19X_3^2 \quad (9)$$

Fig. 12a shows the interactive effects of the side length and depth of the shaped hole on the miss index. The miss index was found to be the lowest when the side length of the shaped hole was at a low level and the depth was at a high level. Given a depth of the shaped hole, the miss index was found to increase rapidly with the decrease of the side length. In contrast, given a side length of the shaped hole, the depth was found to have little effect on the multiples index. Moreover, as shown in Fig. 12b and 12c, the miss index was found to be the lowest when the oblique angle of the shaped hole was at a high level and both the depth and the side length were at low levels.

Table 7 The ANOVA results of the quadratic model response to the miss index

Items	Sum of squares	DOF	Mean square	*F*-value	*p*-value
Model	11.32	9	1.26	26.06	0.0001***
X_1	7.37	1	7.37	152.73	< 0.0001***
X_2	0.82	1	0.82	16.97	0.0045**
X_3	2.51	1	2.51	51.97	0.0002**
$X_1 X_2$	0	1	0	0	1
$X_1 X_3$	0.1	1	0.10	2.12	0.1886
$X_2 X_3$	0	1	0	0	1
X_1^2	0.16	1	0.16	3.22	0.116
X_2^2	0.16	1	0.16	3.22	0.116
X_3^2		1	0.16	3.22	0.116
Residual	0.34	7	0.048		
Lack of fit	0.051	3	0.017	0.24	0.866
Pure error	0.29	4	0.072		

3.1.4 Optimization Analysis and Experimental Validation

To achieve optimal seeding performance, parameter optimization was performed using Design-Expert 8.0 software under the conditions of the factors X_1, X_2, and X_3 with the optimization objects of the highest quality index (Y_1), the lowest multiples index (Y_2), and the lowest miss index (Y_3). The predicted optimization results yielded a quality index of 99.02%, a multiples index of 0.26%, and a miss index of 0.72% when the side length, depth, and oblique angle of the shaped hole were 3.5635 mm, 2.115 mm, and 109.09°, respectively (as shown in Tab. 8). A bench test was performed at Northwest Agriculture & Forestry University in September 2020. In the test, Jingu 21 was used as the experimental material and the rotational speed of the seed-sowing wheel was set as 20 r/min. Under the conditions of the optimized parameters, a total of 100 seed discharging situations was recorded. The simulation and experimental results are reported in Tab. 8. The experimental results were found to be in strong agreement with the simulation results, with a relative deviation of 5.05%. Moreover, the quality index of 94% indicates a good seeding performance under a lower rotational speed of the seed-sowing wheel.

Table 8 The comparison of the simulation test and experimental results

	Side length / mm	Depth / mm	Oblique angle hole / °	Quality index / %	Multiples index / %	Miss index / %
Predicted results	3.5635	2.115	109.09	99.02%	0.26%	0.72%
Simulation results	3.5500	2.100	109.00	99.00%	0.00	1.00%
Experimental results	3.5500	2.100	109.00	94.00%	0.00	6.00%

3.2 Bench Test with Negative Pressure

After the size of the shaped hole was determined, the application of air suction to the seeds in the shaped hole was considered to improve the quality index at a higher rotational speed of the seed-sowing wheel. Four groups of experiments (no negative pressure, −80 Pa, −90 Pa, and −100 Pa) were conducted to compare the seeding performances when the rotational speed of the seed-sowing wheel was increased to 40r/min. A total of 100 seed discharging situations was recorded.

Table 9 The results of the bench test with negative pressure

	Negative Pressure / Pa	Quality index / %	Multiples index / %	Miss index / %
1	0	78	0	22
	80	88	0	12
	90	92	0	8
	100	92	0	8
2	0	75	0	25
	80	86	0	14
	90	91	0	9
	100	93	0	7
3	0	77	0	23
	80	88	0	12
	90	90	0	10
	100	91	0	9

As shown in Tab. 9, at the higher rotational speed of the seed-sowing wheel, the quality index decreased significantly to below 80%, which was accompanied by the significant increase of the miss index. However, when negative pressure was applied to the seeds, the miss index decreased with the increase of the negative pressure, indicating that the air suction could significantly promote

seeds to enter the shaped hole. In contrast, when the negative pressure exceeded −90 Pa, the increase of the negative pressure had no effect on the quality index. Therefore, applying appropriate negative pressure to the seeds was found to improve the quality index at a high rotational speed of the seed-sowing wheel. Under the conditions of a 40 r/min rotational speed of the seed-sowing wheel and negative pressure of −90 Pa, the quality index exceeded 90%.

4 CONCLUSION

In this study, the DEM and RSM were used to research the influences of the side length, depth, and oblique angle of the shaped hole on the seeding performance (quality, multiples, and miss indices) of a seed-metering device, and the parameters of the shaped hole were optimized. Furthermore, after determining the size of the shaped hole, the influence of negative pressure on the quality index was studied under the condition of a higher rotational speed of the seed-sowing wheel. The following conclusions were drawn.

(1) When the rotational speed of the seed-sowing wheel was 20 r/min, the optimal values of the side length, depth, and oblique angle of the shaped hole were respectively 3.55 mm, 2.1 mm, and 109°, which resulted in a quality index of 94%. The optimal parameters were consistent with the simulated and bench test values, with a relative deviation of 5.05%.

(2) Under the conditions of a 40 r/min rotational speed of the seed-sowing wheel, the application of appropriate negative pressure on the seeds was found to promote seed entry into the shaped hole, thus significantly reducing the miss index and increasing the quality index. When the negative pressure was −90 Pa, the quality index could reach more than 90%.

The limitation of this study was that the tests were conducted only under laboratory conditions. Thus, caution should be taken when applying the results.

Acknowledgments

This research was supported by the National Key Research and Development Program (Grant No.2018YFD0701102), the Natural Science Foundation of Ningxia (No. 2023AAC03302) and North Minzu University (Grant No. 2021KYQD31).

5 REFERENCES

[1] Wu, L. & Qu, L. (2018). A review on the resource and processing of the millet. *Food Research and Development*, *39*(15), 191-196.

[2] Zhang, X., Shan, L., Li, Z., Wang, L., & Chai, Y. (2007). The production and distribution of minor crops in the Loess Plateau of China. *Chinese Journal of Eco-Agriculture*, *15*(3), 80-85.

[3] Chen, T., Yi, S., Li, Y., Tao, G., & Mao, X. (2021). Research status and prospect of millet seed-metering device. *Journal of Agricultural Mechanization Research*, *43*(9), 1-6.

[4] Zhang, Y., Zhang, W., & Li, D. (2010). Design for precision metering device with center transmission. *Transactions of the Chinese Society for Agricultural Machinery*, *41*(2), 78-81+121.

[5] Xie, W. & Liu, Y. (2018). Seeding performance of rape seeding device of socket-roller. *Contemporary Farm Machinery*, (10), 67-69.

[6] Li, N., Zhao, M., Liu, F., Liu, Y., Lv, B., Zhang, T., & Chen, C. (2016). Experimental study on the performence of pheumatic precision metering device for millet seeds. *Journal of China Agricultural University*, *21*(5), 122-128.

[7] Zhang, Y., Liu, F., Zhao, M., & Lv, B. (2016). Small size Air-suction seed seedmeter suction hole cleaning device design and simulation. *Journal of Agricultural Mechanization Research*, *38*(11), 23-27.

[8] Kang, S., Ni, X., Qi, Q., Li, S., & Xu, G. (2020). Design and experiment of pneumatic cylinder precision seed-metering device for cotton. *Journal of Agricultural Mechanization Research*, *42*(6), 136-141.

[9] Jia, H., Chen, Y., Zhao, J., Wang, J., Guo, M., & Zhuang, J. (2018). Design and experiment of pneumatic-mechanical combined precision metering device for soybean. *Transactions of the Chinese Society for Agricultural Machinery*, *49*(4), 75-86+139.

[10] Sahoo, P. & Srivastava, A. (2000). Development and performance evaluation of okra planter. J*ournal of Agricultural Engineering*, *37*(2), 15-25.

[11] Chen, Y., Jia, H., Wang, J., Wang, Q., Zhao, J., & Hu, B. (2017). Design and experiment of scoop metering device for soybean high-speed and precision seeder. *Transactions of the Chinese Society for Agricultural Machinery*, *48*(8), 95-104.

[12] Zhang, H., Zhao, J., Hu, G., Bu, L., Wang, Z., Qi, C., & Chen, J. (2020). Parameter optimization of wheat seeding device with nest round wheel. *Journal of Agricultural Mechanization Research*, *42*(9), 139-144.

[13] Liu, X., Chen, K., Wang, X., He, X., & Li, W. (2022). Parameter optimization for a potato rod-type conveyor grading device based on the discrete element method. *Tehnicki Vjesnik-Technical Gazette*, *29*(4), 1354-1361. https://doi.org/10.17559/TV-20210726055221

[14] Pasha, M., Hare, C., Ghadiri, M., Gunadi, A., & Piccione, P. M. (2016). Effect of particle shape on flow in discrete element method simulation of a rotary batch seed coater. *Powder Technology*, *296*, 29-36. https://doi.org/10.1016/j.powtec.2015.10.055

[15] Bertrand, F., Leclaire, L. A., & Levecque, G. (2005). DEM-based models for the mixing of granular materials. *Chemical Engineering Science*, *60*(8-9), 2517-2531. https://doi.org/10.1016/j.ces.2004.11.048

[16] Bu, L., Hu, G., Chen, C., Sugirbay, A., & Chen, J. (2020). Experimental and simulation analysis of optimum picking patterns for robotic apple harvesting. *Scientia Horticulturae*, *261*, 108937. https://doi.org/10.1016/j.scienta.2019.108937

[17] Xue, P., Xia, X., Gao, P., Ren, D., Hao, Y., Zheng, Z., & Huang, Y. (2019). Double-setting seed-metering device for precision planting of soybean at high speeds. *Transactions of the ASABE*, *62*(1), 187-196. https://doi.org/10.13031/trans.13055

Contact information:

Qianwen KOU
North Minzu University,
Yinchuan, Ningxia, 750021, China
E-mail: kouqianwen2023@126.com

Lingxin BU
(Corresponding author)
College of Mechatronic Engineering, North Minzu University,
Yinchuan, Ningxia, 750021, China
E-mail: 2021023@nmu.edu.cn

Jun CHEN,
College of Mechanical and Electronic Engineering,
Northwest A & F University Yangling,
Shaanxi, 712100, China
E-mail: chenjun_jdxy@nwsuaf.edu.cn

Adilet SUGIRBAY
Technical faculty, S. Seifullin Kazakh Agro Technical University,
Astana 010000, Kazakhstan
E-mail: sugirbayadilet@nwafu.edu.cn